Raman shifter optimized for lidar at a 1.5 μm wavelength

Scott M. Spuler and Shane D. Mayor

A Raman shifter is optimized for generating high-energy laser pulses at a 1.54 μm wavelength. A forward-scattering design is described, including details of the multiple pass and nonfocused optical design, Stokes injection seeding, and internal gas recirculation. First-Stokes conversion efficiencies up to 43%—equivalent to 62% photon conversion efficiency—were measured. Experimental results show output average power in excess of 17.5 W, pulse energies of 350 mJ at 50 Hz, with good beam quality ($M^2 < 6$). Narrow bandwidth and tunable output is produced when pumping with a single longitudinal mode Nd:YAG laser and seeding the process with a Stokes wavelength narrowband laser diode. © 2007 Optical Society of America

OCIS codes: 010.3640, 280.3640, 140.3550, 280.1100, 280.1120.

1. Introduction

Stimulated Raman scattering (SRS) in methane is a well-known and popular method for generating laser radiation at a 1.5 μm wavelength. The ability to produce high-energy pulses in a region of the spectrum that offers maximum eye safety[1]—as shown in Fig. 1—is particularly attractive for applications such as lidar.[2–5] Unfortunately, traditional Raman shifting to convert 1 μm pump radiation to 1.5 μm has required frequent optics cleaning, provided poor beam quality, and has limited pulse repetition frequency (PRF). As a result of these problems, the technique is understandably dismissed by many searching for a reliable lidar transmitter at this wavelength.[6] In this paper, we present results that demonstrate that it is possible to overcome these problems and offer new hope for the use of Raman shifters in advanced lidar applications in this wavelength region.

Briefly described, Raman scattering occurs when a photon is inelastically scattered from a molecule leaving both the molecule in an excited state and the photon wavelength shifted. If the intensity of the incident beam is very high, the initially scattered photons can further enhance the process and lead to stimulated Raman scattering. In this nonlinear optical process, the Stokes field is amplified with energy transferred from the pump laser when the frequency difference between the two coherent fields match the frequency of the Raman active medium.

2. Design Considerations

Historically, for efficient stimulated Raman scattering in methane, high-energy lasers were tightly focused inside pressurized cells.[7] The high-energy density from these focused-geometry cells often led to laser-induced breakdown, which was shown to be a factor limiting the conversion efficiency and the quality of the Stokes beams.[8] Furthermore optical breakdown of methane led to soot deposits, potentially damaging the Raman cell optics, and required frequent cleaning.[5,9,10] Experiments have shown H_2:CH_4 mixtures have higher photochemical stability when compared with pure methane;[11] however, soot formation can be most effectively eliminated by reducing the energy density of the pump beam.[12–14] Efficient SRS conversion with reduced pump intensity is possible by increasing the interaction length with a folded cell geometry.[12,13] This approach greatly improves the reliability of CH_4 Raman shifters, making them suitable for long-term operation. Additionally, the reduced pump intensity of multipass geometries has been shown to suppress processes such as higher-order Stokes, anti-Stokes, and backward Stokes.[15] And, since the transit time of the pump through the cell is configured to be greater than the temporal width of the pump, the growth of backward Stokes is greatly reduced.[16]

An additional past problem in high-energy methane Raman cells included damage to optical coatings of the cell windows and internal optics. The inner

The authors are with the National Center for Atmospheric Research, Earth Observing Laboratory, P.O. Box 3000, Boulder, Colorado 80307-3000. The e-mail address for S. D. Mayor is shane@ucar.edu.

Received 4 December 2006; accepted 23 December 2006; posted 12 January 2007 (Doc. ID 77724); published 1 May 2007.
0003-6935/07/152990-06$15.00/0

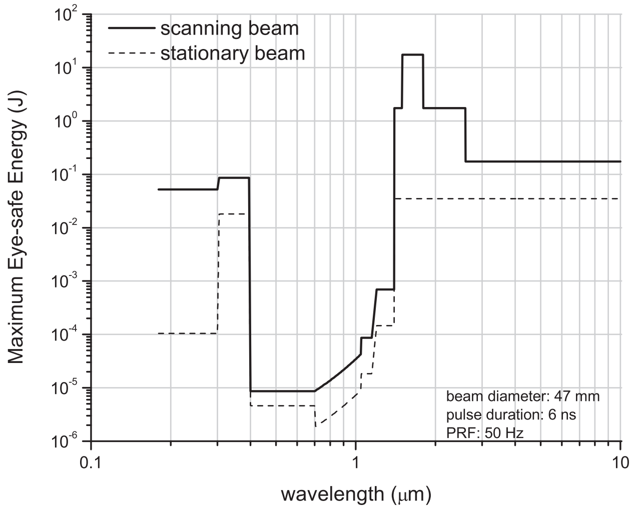

Fig. 1. (Color online) Maximum eye-safe energy versus wavelength as calculated by American National Standard for Safe Use of Lasers, ANSI Z136.1-2000, for the conditions shown. The solid curve is calculated for a single shot exposure. The dashed curve is calculated for multiple shots, or stationary laser beam conditions, with exposure times based on the natural aversion time of the human eye: 0.25 s and 10 s for inside and outside the visible wavelength region, respectively.

faces of the antireflection coated cell windows were often etched at the exact location of the laser spot. This effect has been attributed to the laser-induced generation of reactive radicals. A simple solution to this problem is to use cell windows with no coatings. Another approach, and perhaps more elegant with higher throughput, utilizes uncoated windows at the Brewster angle. Similarly, the high-reflection (HR) coatings of internal cell mirrors used to fold the beam path were vulnerable to damage. Hot spots in the pump beam, flaws in the HR coatings, or particles on the mirror surface could cause sudden failure of the mirror during operation. To avoid this problem, the mirrors were replaced with prisms to reverse and translate the beam by total internal reflection. The prisms are designed so that the beam enters and exits at the Brewster angle—therefore eliminating the need for an antireflecting coating. The absence of all optical coatings dramatically increases the durability of the Raman shifter. The prism and window substrate material—Infrasil—was selected for its low dispersion properties. This design feature is required in order to keep the pump and Stokes beam overlapped throughout the entire interaction length. The glass also has negligible absorption at 1.5 μm due to low OH content. The cell windows are 50 mm in diameter by 12.5 mm thick.

The Raman cell with the design features described herein performs its wavelength conversion function most efficiently when the pump beam is linearly polarized. Due to the Brewster angle interface of all the optics, the cell is essentially lossless for P polarization. Whereas, the total transmission for S polarization is 20.5% (12 surfaces with the transmission at each surface of 87.6%). Also, the polarization is preserved for the first Stokes shift in CH_4 because of the symmetry of the υ_1 vibration (symmetrical stretch). As a result, this Raman cell design is useful for generating high polarization purity output of the Stokes radiation. This is a desirable characteristic for use in the polarization lidar technique.[17,18]

The limitation of higher PRF with methane Raman shifters is due to a local heating effect. During the conversion process, energy is deposited in the gas in the form of vibrational excitation equivalent to the difference in energy between the converted pump photons and Stokes photons. The vibrationally excited molecules quickly convert this energy to heat resulting in temperature fluctuations in the gas. This leads to distortions in the optical beams since the index of refraction of the gas is a function of temperature. In the absence of mechanical or convective mixing, the speed at which the distortions dissipate is inversely related to the thermal conductivity of the gas. The lower thermal conductivity of CH_4 compared with H_2 and D_2 limits the maximum repetition rate of the pump laser beam.[11] It has been shown that without gas circulation, there is considerable optical distortion in the beam path, which degrades Raman conversion efficiency.[9] The cell characterized herein employs a simple yet effective method to circulate the methane. Internal circulation is provided by an array of low-cost axial fans. The cell mechanical design includes internal shrouding and flow straighteners to minimize index changes from turbulence. Furthermore, the flow is transverse to the beam plane to minimize the distance the heated gas must travel before the next laser pulse arrives. Figure 2 shows a semitransparent solid model of the cell. It is approximately 80 cm long by 20 cm in diameter and weighs 30 kg.

Without an external seed, the Stokes field is initiated by spontaneously emitted photons. This stochastic process causes the energy and spatial characteristics of the output beam to fluctuate. Seeding of Raman amplifiers has been shown to stabilize the Stokes output.[19] Previously, we performed tests with a broadband Nd:YAG pump laser while seeding with a cw, narrowband, distributed feedback (DFB) laser at the first Stokes frequency. These experiments resulted in improved conversion efficiency, especially at

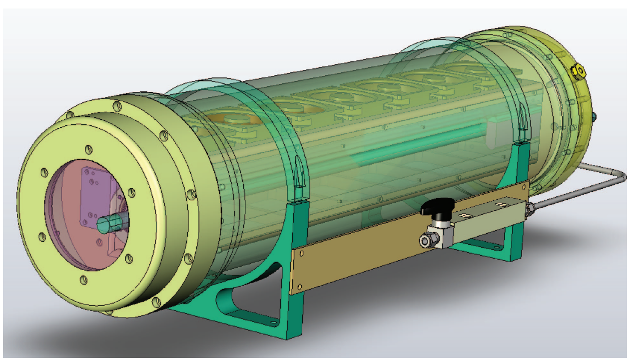

Fig. 2. Semitransparent solid model of the Raman cell.

lower gas pressures.[13,20] This paper describes additional experiments using both broadband and narrowband Nd:YAG pump lasers with a similar Stokes seeding technique.

3. Experimental Results

A. Optimization of Stokes Conversion Efficiency and Beam Quality at 10 Hz

The first experimental arrangement used a pump beam from a 10 Hz Q-switched Nd:YAG laser (Continuum Surelite III) at 1064 nm with a pulse width of 6 ns. An optical isolator was used to protect the laser from backscattered light. Following the isolator, the pump beam was linearly polarized resulting in approximately 615 mJ per pulse. The experimental layout is shown in Fig. 3. The first-Stokes SRS process was seeded with a cw diode laser (ThorLabs WDM8-C-33A-20-NM) with a specified center wavelength stability of better than 0.002 nm per 24 h. The Stokes seed beam was matched to the pump laser input diameter and overlapped in space as well as wavelength matched to the Stokes centerline. The Stokes output from the Raman cell was separated from the residual pump and any four-wave mixing (FWM) using a combination of a dichroic mirror and high dispersion Pellin Broca prism.

The pump beam diameter of 9 mm was reduced with a lens set to increase the energy density of the beam prior to entering the Raman shifter. A range of lens sets was explored to determine the influence of different pump beam geometries (i.e., slight convergence, divergence, and entrance beam diameter) on the SRS conversion efficiency. It was found that roughly matching the fluence at the input and output of the cell produced the highest conversion efficiency. As the pump beam was heavily depleted at greater distances through the cell, this required a slightly converging beam to maintain the same fluence throughout the cell. The optimal fluence was estimated at approximately 1.7 J/cm^2, assuming a Gaussian intensity profile. The true profile and variations (e.g., hot spots) were not accounted for in this estimate. The optimal lens arrangement placed the theoretical pump beam-waist radius (1 mm) approximately 2 m beyond the exit of the cell (note: the path inside the cell is approximately 3 m). Initial measurements of the beam quality showed the Stokes output to have an M^2 of 15. The pump beam was somewhat oval in shape in the far field (a result of the particular pump laser), so a 5 m focal length cylindrical lens was added to make the beam shape more circular. This produced Stokes output with an M^2 of 11, while achieving conversion efficiencies of up to 37% at pressures from 8.2 to 13 atm. The quantum or photon conversion efficiency in this case would be 54% since one 1064 nm photon is annihilated to create another at 1543 nm.

To further improve the Stokes beam quality, argon gas was mixed with methane as a buffer gas. The buffer gas increases the wave-vector mismatch thereby decreasing the FWM efficiency.[11,21] At active gas pressures of 6–7 atm and buffer gas pressures of 5–6 atm, the Stokes beam quality was measured at an M^2 of 7. At these reduced pressures, there was a slight (~5%) reduction in conversion efficiency from the peak. However, there was a strong dependence on Stokes seeding to maintain conversion efficiency and suppress FWM. When the Stokes seed was blocked, the pump beam fluence increased—due to reduced

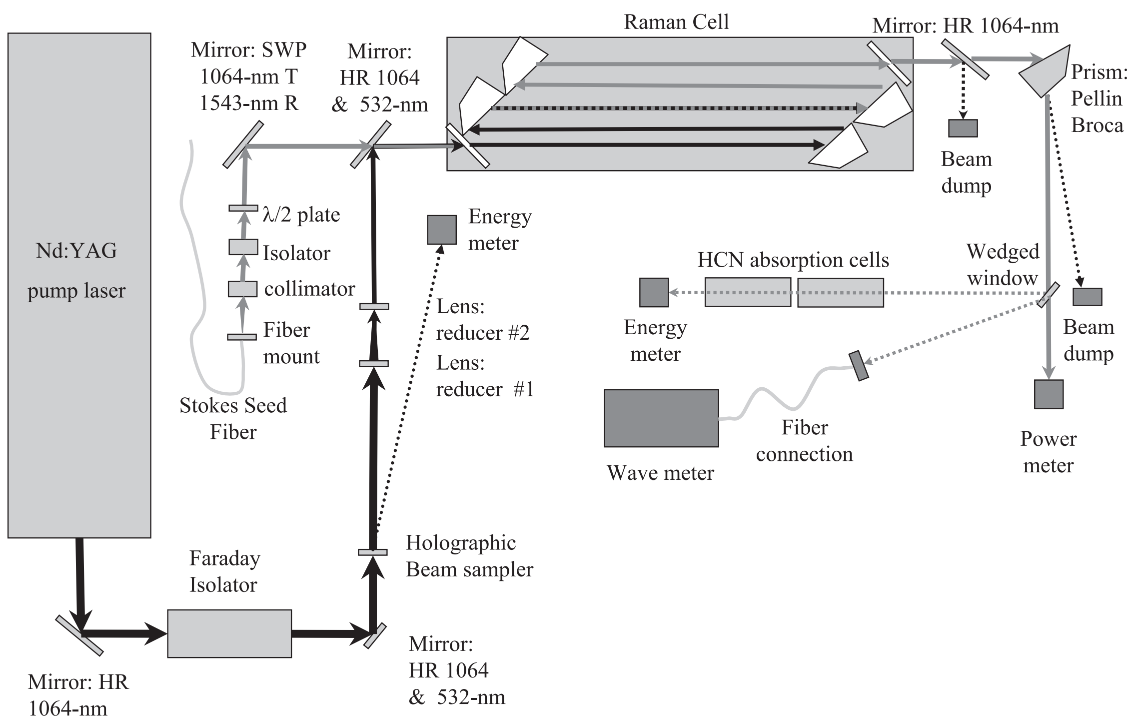

Fig. 3. Experimental layout.

conversion efficiency—which damaged optical components of the cell and subsequent optics. As a compromise of reliability, beam quality, and conversion efficiency, a mixture of 9.5 and 4.1 atm partial pressures of CH_4 and Ar, respectively, was selected. This mixture produced a Stokes conversion efficiency of 35% with an M^2 of 9.

Following these optimization tests, the Raman shifter was installed as part of an eye-safe lidar system for a field operation over a 4 week period. The cell, pumped with the Nd:YAG laser described above was operated for over 100 h. At the end of the experiment, the optics were carefully examined and showed no trace of contamination or damage. Furthermore, the Raman shifter was able to maintain the stringent pointing stability requirements (<100 μrad) of the lidar instrumentation throughout the entire project without realignment.[18] More recently, the reliability of the design has been demonstrated in a system with an identical Raman shifter for a specific application.[22] The device has demonstrated reliable operation for >7 months.

B. Conversion Efficiency and Beam Quality at Higher Pulse Repetition Frequency Using a Narrowband Nd:YAG Pump

In the next phase of the experiment, the pump laser was replaced with a 50 Hz Q-switched Nd:YAG laser (Continuum Powerlite 9050) with a pulse width of 9 ns. The laser is injection seeded with a single frequency fiber laser module with thermal wavelength tuning for single-longitudinal-mode operation. Following the isolator, the pump beam was linearly polarized with ~905 mJ per pulse.

Stokes conversion efficiencies and beam quality were measured pumping the cell at PRFs ranging from 10 to 50 Hz. Stokes pulse energies of up to 390 mJ/pulse were measured with a 6 ns duration. Conversion efficiencies of 43% to 38% were measured from 10 to 50 Hz, respectively. The beam quality, M^2 parameter, was less than 6 at all PRFs. The results are shown in Fig. 4. As a note, the pump beam convergence was increased at higher repetition rates to maintain high conversion efficiencies. This was likely required due to increased thermal lensing at the higher pulse rates and may be responsible for the slight improvement in beam quality. For all PRFs, the beam convergence was set just below the threshold where backward SRS was detectable with an IR-sensitive card at the dichroic mirror where the Stokes seed and pump beam are overlapped.

C. Stokes Linewidth Using a Narrowband Pump Laser

A Fizeau interferometer-based wavelength and linewidth meter (High Finesse WS-7 IR) were used to measure the spectral properties of the laser outputs. As shown in the experimental layout, Fig. 3, a small fraction of the Stokes beam was reflected off an uncoated wedged window and focused onto a single-mode fiber, which was connected to the interferometer. The wavelengths of the fiber-coupled Nd:YAG pump seed

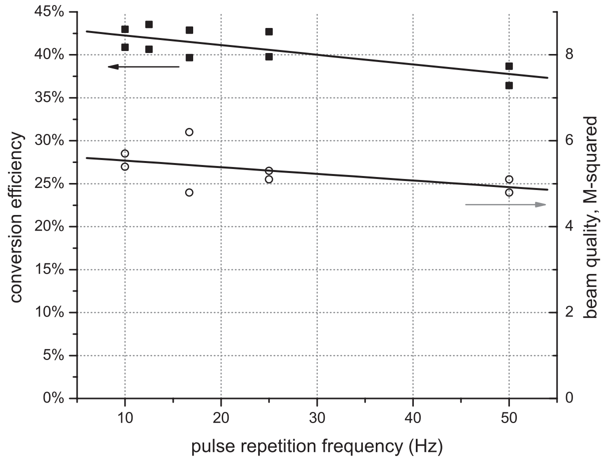

Fig. 4. Experimental results of conversion efficiency (solid squares) and beam quality (open circles) as a function of pulse repetition frequency.

and Stokes seed were monitored using fibers with a 1% tap fed into the Fizeau interferometer via an optical fiber switcher.

For a pump wavelength of 1064 nm, the FWHM Raman linewidth, $\Delta\nu_S$, in methane can be calculated according to the following empirical formula given in Ref. 23:

$$\Delta\nu_S(p) = 8.7 + 0.39p \quad (\text{GHz}), \tag{1}$$

where p is the methane pressure in atmospheres. Equation (1) predicts a Raman linewidth of 12.7 GHz at a pressure of 10.2 atm. However, as discussed in the literature,[24,25] when the laser bandwidth is much smaller than the Raman linewidth, and when the gain is high, line narrowing occurs by amplifying the center part of the Stokes line more strongly than the wings. The gain narrowed Stokes linewidth is given by[26]

$$\Delta\nu_{S,gn}(p) = \Delta\nu_S(p)\sqrt{\ln(2)/\ln(E_f/E_i)}, \tag{2}$$

where E_i and E_f are the initial and final Stokes energy. Assuming an initial Stokes energy equal to one spontaneously emitted photon ($E_i = hc/\lambda_S$), and the final Stokes energy of ~300 mJ, Eq. (2) predicts a gain narrowed linewidth of approximately 1.6 GHz FWHM. Without Stokes seeding, the output Stokes beam was measured to have a bandwidth of approximately 1.3 GHz (10.0 pm), which is in reasonable agreement with the expected gain-narrowed linewidth.

The Raman linewidth is important when generating SRS from spontaneous emission. However, when seeding the process, the output linewidth is determined by a combination of the pump and the Stokes seed linewidth. In this case, the Stokes seed is a narrow diode with a bandwidth of <10 MHz, so the pump will dominate the bandwidth. Therefore, assuming efficient seeding, we expect the SRS output linewidth to be similar to the pump bandwidth. With

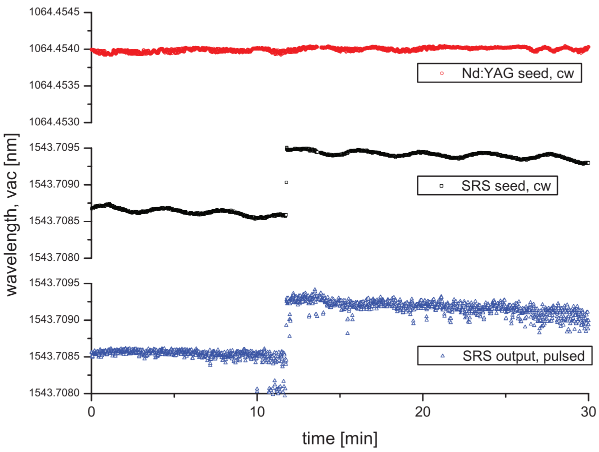

Fig. 5. (Color online) Experimental measurement of pump seed, Stokes seed, and Stokes output wavelengths over a 30 min period. The Stokes seed was tunable in 1 pm steps and was adjusted up 1 pm at approximately the 12 min point in the plot.

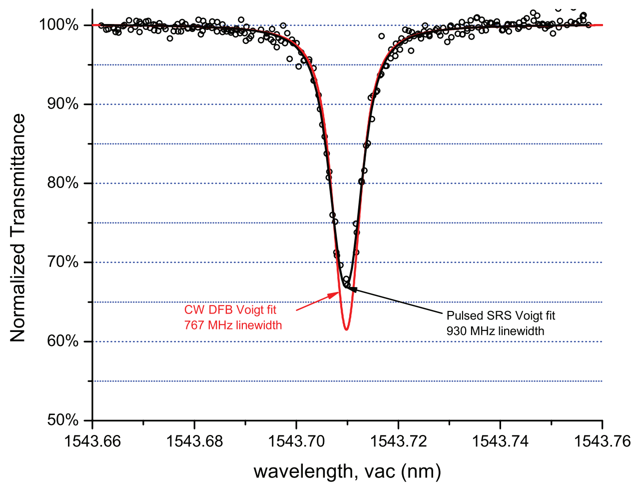

Fig. 6. (Color online) Transmission of the pulsed Stokes output scanning across a 5 Torr $H^{12}CN$, P(13) line (circles). A Voigt fit is shown as a solid black line. A reference curve (solid gray line, online version is red) was measured by scanning over the feature with a cw DFB laser.

~5 mW of Stokes seeding at 1543.817 nm and pumping at 1064.500 nm, the Stokes linewidth was measured with the Fizeau interferometer to be 210 ± 34 MHz (1.67 ± 0.27 pm) with a center wavelength 1543.807 nm. This value is in reasonable agreement with the expected Stokes seed narrowed linewidth since the pump laser has an ~100 MHz bandwidth.

To further investigate the Stokes linewidth and demonstrate limited wavelength agility, the output of the Raman cell was tuned across a molecular absorption feature. To change the wavelength of the SRS output, the Stokes seed wavelength was adjusted in 1 pm increments via computer control. Due to the slow response time of the thermal wavelength tuning of the pump fiber laser seed module, it was adjusted to maintain resonance with the methane—with a center Raman shift of 2916.58 cm^{-1}—in 5–10 pm steps during the scan. All three center wavelengths, Stokes seed, pump seed, and Stokes output, were monitored in real time via the optical switch into the Fizeau interferometer. Figure 5 shows these three signals measured over a 30 min time span.

As shown in the experimental setup, Fig. 3, a small fraction of the Stokes output beam was passed through a pair of 10 cm length absorption cells containing 5 Torr of $H^{12}CN$ each (Wavelength References model: HCN-12-T-5). The experiment targeted the $2\nu_3$ rotational-vibrational band, specifically the P(13) line, which has a center wavelength of 1543.709 nm. The transmission of Stokes output at each wavelength step is shown in Fig. 6 as open circles—each point represents a 30 s average. The result was fit with a Voigt function, which has a measured linewidth of 930 MHz. This function is a convolution of the absorption feature and the Stokes output linewidth. To measure the absorption feature with minimal influence of a laser bandwidth, the narrowband cw DFB Stokes seed laser was tuned over the absorption feature. This reference curve is shown in Fig. 6 as a solid gray line. The linewidth of the feature was measured to be ~770 MHz FWHM. This value is in general agreement with theory, assuming the feature has a broadening coefficient of approximately 80 MHz/Torr[27] and room temperature Doppler broadening of ~460 MHz. To estimate the linewidth of the pulsed Stokes output, the convolution of the cw DFB Voigt fit with a Lorentz function (representing the laser line shape) was calculated and the Lorentzian width adjusted to match the pulsed SRS output Voigt fit. By this method, the linewidth of the Stokes output is estimated to be approximately 164 MHz. This inferred value is in close agreement with that measured by the interferometer.

4. Conclusions

This paper describes the optimization and characterization of a Raman shifter designed for high-energy laser pulse applications. Field operation of the device over extended periods of time proves the traditional problem of breakdown and sooting, and optical coating degradation has been addressed. Laboratory results using a narrowband pump show that conversion efficiencies of ~40% are obtained with good beam quality at PRFs up to 50 Hz. We intend to use these features to build more efficient and reliable eye-safe lidar systems with longer range and faster scanning capability.

In addition to improved conversion efficiency and reliability, it was shown that the Stokes pulses have narrow linewidth with limited tunability. If the Stokes line center is stabilized, these spectral features are potentially significant for advanced lidar applications. For example, by using different gases and or pump wavelengths,[28] it may be possible to perform differential absorption lidar[29,30] (DIAL) for important atmospheric species such as water vapor. Furthermore, by constructing a long path-length notch filter using HCN in a receiver, it would be possible to separate molecular from aerosol backscatter. Although molecular backscattering is weak at this wavelength, approximately

$10^{-8}\ m^{-1}\ sr^{-1}$, we estimate there is sufficient signal with a high pulse energy lidar for calibration out to several kilometers. This technique, known as high spectral resolution lidar[31] (HSRL), allows one to remotely measure aerosol properties such as optical depth and backscatter coefficients. We are in the process of evaluating the possibility of applying the HSRL technique at this wavelength region for scanning lidar applications.

The development of the Raman cell was funded by the 2002 NCAR Director's Opportunity fund and the Earth Observing Laboratory. We thank Tomás Avilez for assistance with laboratory testing and Karl Schwenz for the mechanical design of the Raman cell.

References

1. American National Standard for the Safe Use of Lasers, "Standard for the safe use of lasers," Tech. Rep. ANSI Z136.1-2000 (America American National Standards Institute, 2000).
2. E. M. Patterson, D. W. Roberts, and G. G. Gimmestad, "Initial measurements using a 1.54 micron eyesafe Raman shifted lidar," Appl. Opt. **28,** 4978–4981 (1989).
3. W. Carnuth and T. Trickl, "A powerful eyesafe infrared aerosol lidar: application of stimulated Raman backscattering of 1.06 micron radiation," Rev. Sci. Instrum. **65,** 3324–3331 (1994).
4. G. Roy and P. Mathieu, "Comparison of Raman and degenerated optical parameteric oscillators for a high-energy and high-repetition-rate eye-safe laser," Opt. Eng. **35,** 3579–3584 (1996).
5. J. D. Spinhirne, S. Chudamani, J. F. Cavanaugh, and J. L. Bufton, "Aerosol and cloud backscatter at 1.06, 1.54, and 0.53 microns by airborne hard-target-calibrated Nd:YAG/methane Raman lidar," Appl. Opt. **36,** 3475–3490 (1997).
6. V. A. Kovalev and W. E. Eichinger, *Elastic Lidar* (Wiley, 2004).
7. D. J. Brink, H. P. Burger, T. N. de Kock, J. A. Strauss, and D. R. Preussler, "Importance of focusing geometry with stimulated Raman scattering of Nd:YAG laser light in methane," J. Phys. D **19,** 1421–1427 (1986).
8. L. de Schoulepnikoff, V. Mitev, V. Simeonov, B. Calpini, and H. van den Bergh, "Experimental investigation of high-power single pass Raman shifters in the ultraviolet with Nd:YAG and KrF lasers," Appl. Opt. **36,** 5026–5042 (1997).
9. R. Stultz, D. E. Nieuwsma, and E. Gregor, "Eyesafe high pulse rate laser progress at hughes," in *Eyesafe Lasers: Componets, Systems, and Applications,* Proc. SPIE **1419,** 64–74 (1991).
10. M. J. Shaw, J. P. Partanen, Y. Owadano, I. N. Ross, E. Hodgson, C. B. Edwards, and F. O'Neill, "High-power forward Raman amplifiers employing low-pressure gases in light guides. II. Experiments," J. Opt. Soc. Am. B **3,** 1466–1475 (1986).
11. V. Simeonov, V. Mitev, H. van de Bergh, and B. Calpini, "Raman frequency shifting in a CH_4:H_2:Ar mixture pumped by the fourth harmonic of a Nd:YAG laser," Appl. Opt. **37,** 7112–7115 (1998).
12. N. A. Kurnit, R. F. Harrison, R. R. Karl, Jr., J. P. Brucker, J. Busse, W. K. Grace, O. G. Peterson, W. Baird, and W. S. Hungate, "Generation of 1.54 micron radiation with application to an eye-safe laser lidar," in *Proceedings of the International Conference on LASERS '97,* S. Press, ed. (McLean, 1998), pp. 608–610.
13. S. D. Mayor and S. M. Spuler, "Raman-shifted eye-safe aerosol lidar," Appl. Opt. **43,** 3915–3924 (2004).
14. P. Maroni, D. Papageorgopoulos, A. Ruf, R. D. Beck, and T. R. Rizzo, "Efficient stimulated Raman pumping for quantum state resolved surface reactivity measurements," Rev. Sci. Instrum. **77,** 054103 (2006).
15. D. C. MacPherson, R. C. Swanson, and J. L. Carlsten, "Stimulated Raman scattering in the visible with a multipass cell," IEEE J. Quantum Electron. **25,** 1741–1746 (1989).
16. P. R. Battle, J. G. Wessel, and J. L. Carlsten, "Gain-guiding effects in an amplifier with focused gain," Phys. Rev. A **48,** 707–716 (1993).
17. K. Sassen, "The polarization lidar technique for cloud research: a review and current assessment," Bull. Am. Meteorol. Soc. **72,** 1848–1866 (1991).
18. S. D. Mayor, S. M. Spuler, and B. M. Morley, "Scanning eye-safe depolarization lidar at 1.54 microns and potential usefulness in bioaerosol plume detection," in *Lidar Remote Sensing for Environmental Monitoring IV* (Society of Photo-Optical Instrumentation Engineers, 2005).
19. J. G. Wessell, K. Repasky, and J. L. Carlsten, "Competition between spontaneous scattering and stimulated scattering in an injection-seeded Raman amplifier," Phys. Rev. A **53,** 1854–1860 (1996).
20. S. M. Spuler and S. Mayor, "Scanning eye-safe elastic backscatter lidar at 1.54 microns," J. Atmos. Ocean. Technol. **22,** 696–703 (2005).
21. L. Schoulepnikoff and V. Mitev, "High-gain single pass stimulated Raman scattering and four-wave mixing in a focused beam geometry: a numerical study," Pure Appl. Opt. **6,** 277–302 (1997).
22. T. Warner, P. Benda, S. Swerdlin, J. Knievel, E. Argenta, B. Aronian, B. Balsley, J. Bowers, R. Carter, P. A. Clark, K. Clawson, J. Copeland, A. Crook, R. Frehlich, M. L. Jensen, Y. Liu, S. Mayor, Y. Meillier, B. Morley, R. Sharman, S. Spuler, D. Storwold, J. Sun, J. Weil, M. Xu, A. Yates, and Y. Zhang, "The pentagon shield program toward critical infrastructure protection," Bull. Am. Meteor. Soc. **88,** 167–176, doi:10.1175/BAMS-88-2-167 (2007).
23. A. Kazzaz, S. Ruschin, I. Shoshan, and G. Ravnitsky, "Stimulated Raman scattering in methane—experimental optimization and numerical model," IEEE J. Quantum Electron. **30,** 3017–3024 (1994).
24. C. S. Wang, "Theory of Raman scattering," Phys. Rev. **182,** 482–494 (1969).
25. M. G. Raymer and J. Mostowski, "Stimulated Raman scattering: unified treatment of spontaneous initiation and spatial propagation," Phys. Rev. A **24,** 1980–1992 (1981).
26. D. C. MacPherson, R. C. Swanson, and J. L. Carlsten, "Quantum fluctuations in the stimulated-Raman-scattering linewidth," Phys. Rev. Lett. **66,** 66–69 (1988).
27. W. C. Swann and S. L. Gilbert, "Line centers, pressure shift, and pressure broadening of 1530–1560 nm hydrogen cyanide wavelength calibration lines," J. Opt. Soc. Am. B **22,** 1749–1756 (2005).
28. X. Hua, J. Leng, H. Yang, G. Sha, and C. Zhang, "Highly efficient Raman conversion on O_2 pumped by a seeded narrow band second-harmonic Nd:YAG laser," Appl. Phys. B **81,** 525–530 (2005).
29. G. G. Gimmestad, "Differential-absorption lidar for ozone and industrial emissions," in *Lidar,* C. Weitkamp, ed. (Springer, 2005), pp. 187–212.
30. J. Bösenberg, "Differential-absorption lidar for water vapor and temperature profiling," in *Lidar,* C. Weitkamp, ed. (Springer, 2005), pp. 213–239.
31. E. W. Eloranta, "High spectral resolution lidar," in *Lidar,* C. Weitkamp, ed. (Springer, 2005), pp. 143–163.